ANALYTICAL BIOCHEMISTRY **252,** 217–228 (1997)
ARTICLE NO. AB972326

BIACORE Analysis of Histidine-Tagged Proteins Using a Chelating NTA Sensor Chip

Lars Nieba,* Sabine E. Nieba-Axmann,* Anette Persson,† Markku Hämäläinen,† Fredrik Edebratt,† Anna Hansson,† Jonas Lidholm,‡ Kjell Magnusson,† Åsa Frostell Karlsson,†,[1] and Andreas Plückthun*,[1]

**Biochemisches Institut der Universität Zürich, Winterthurerstrasse 190, CH-8057 Zürich, Switzerland; †Biacore AB, S-75450 Uppsala, Sweden; and ‡Pharmacia Diagnostics, S-75182 Uppsala, Sweden*

Received January 28, 1997

While BIACORE instruments are routinely used for kinetic measurements and for the determination of binding constants, the immobilization of a ligand onto the sensor chip surface has to be individually optimized for every system. We show here that the histidine (His) tag, routinely used in protein purification and in detection is an ideal tag for immobilization, despite the intrinsically low affinity between an immobilized metal ion and the His tag. This is due to strong rebinding effects caused by the high surface density of immobilized Ni^{2+}–nitrilotriacetic acid (NTA) on the chips used here. The immobilization of the ligand can be adjusted to a low level using the same chip, such that mass transport limitation and rebinding of the analyte to the immobilized ligand is minimal. Nine different proteins with different numbers of His tags were tested for stable binding to the Ni^{2+}–NTA surface. Most proteins with one His tag dissociate very rapidly from the Ni^{2+}–NTA surface, and the K_D for the interaction between His tag and Ni^{2+}–NTA was estimated to about 10^{-6} M at neutral pH. In contrast, two His tags are usually found to be sufficient for stable binding. The kinetics of the chaperonin system of *Escherichia coli* GroEL and GroES were analyzed as a model using this system and found to be very similar to those obtained with covalently immobilized ligands. The sensor chip can be reused many times, because of the powerful regeneration methods. The ligand can be freshly immobilized after each cycle, thus eliminating potential denaturation upon regeneration as a source of error.

Key Words: **BIACORE; IMAC; His tag; GroEL; GroES.**

The advent of tag sequences in protein science (1) has been instrumental for the efficient manipulation of recombinant proteins, notably their purification and detection. One of the most widely used tags is the histidine (His) tag, which typically consists of five or six consecutive His residues (2, 3) added to the C- or N-terminus of the protein. Its imidazole moieties can chelate the free coordination sites of metal ions which are themselves immobilized as chelate complexes of iminodiacetic acid (IDA)[2] or nitrilotriacetic acid (NTA) bound to a solid support (2–4). Typically Ni^{2+}, Zn^{2+}, Co^{2+}, and Cu^{2+} chelated to IDA or NTA have been used in chromatographic media for immobilized metal affinity chromatography (IMAC) (2, 5). The choice of the metal ion and buffer conditions for IMAC are optimized for the highest selectivity relative to other proteins not carrying the His tag, which does not necessarily give the tightest binding of the His tag. A growing range of additional applications rely on the same interaction mechanism for detection of His-tagged molecules (6). Furthermore, recombinant antibodies are now available that recognize the His tag (7).

One of today's front lines in biology is to investigate macromolecular interactions in a quantitative way. Such analyses using BIACORE instruments have been established as a powerful technique. The BIACORE system is a biosensor instrument employing surface plasmon resonance detection for interaction studies (8). With one molecular species (the ligand) immobilized onto a sensor chip, a binding partner in solution (the

[1] To whom correspondence should be addressed. For AFK, fax: (+46)-18-15 01 13. E-mail: asa.frostellkarlsson@eu.biacore.com. For AP, fax: (+41-1)635 5712. E-mail: plueckthun@biocfebs.unizh.ch.

[2] Abbreviations used: CS, citrate synthase; EDTA, ethylenediaminetetraacetic acid; FITC, fluorescein isothiocyanate; GST, glutathione *S*-transferase; HBS, Hepes-buffered saline; IMAC, immobilized metal ion affinity chromatography; IPTG, isopropyl-β-D-thiogalactopyranoside; MBP, maltose-binding protein; Mops, 4-morpholinepropanesulfonic acid; NTA, nitrilotriacetic acid; RU, resonance units; SA, streptavidin; wt, wildtype.

0003-2697/97 $25.00

analyte) can bind to the ligand. This event is continuously monitored and displayed in a sensorgram, where the progress of the interaction is plotted against time, revealing the binding characteristics. Analysis of binding kinetics and affinity as well as mechanisms and stoichiometries for formation of multimolecular complexes are examples of studies that can be achieved in a short time and with small amounts of sample that do not need to be labeled or even purified (8–15). By combining this methodology with His tags, significant advantages in ease and general applicability are apparent (16–19).

In this paper we describe the analysis, characteristics, and usage of a new chelating sensor chip which has NTA preimmobilized to a dextran matrix. An optimized protocol is reported that gives robust and reproducible performance with respect to ligand immobilization and regeneration. The protocol also addresses the need to prevent metal ion contamination by incorporating EDTA as a metal ion scavenger. Immobilization performance is investigated with several proteins of different oligomerization states that carry His tags.

To illustrate the usefulness of the chelating sensor chip in studying biological interactions, we have used it for studies of the *Escherichia coli* chaperonin system. It consists of the two proteins GroEL and GroES (20), which facilitate protein folding in the cell in an ATP-dependent reaction cycle. In this study, His-tagged GroES was utilized, and kinetics of the nucleotide-dependent binding to and dissociation from GroEL were measured. GroEL is a large oligomeric complex composed of two stacked heptameric rings of identical 57-kDa subunits (21, 22). The chaperone function of GroEL is regulated by GroES, which is a single heptameric ring of 10-kDa subunits (23). In the presence of adenine nucleotides, GroEL and GroES oligomers form asymmetric 1:1 complexes, where GroES caps the cavity of one ring of GroEL, leaving the cavity in the other ring open (24). The binding affinity of GroEL for the GroES molecule is very high (25, 26), but the second binding site has low affinity under physiological conditions (27).

MATERIALS AND METHODS

Instrumentation. BIACORE 2000, BIACORE with an installed Upgrade system, and Sensor Chip NTA from Biacore AB were used.

Reagents. $NiCl_2$ and ATP were from Sigma, and ADP, EDTA disodium salt, and all other chemicals were obtained from Fluka. Enzymes were obtained from New England Biolabs and Boehringer-Mannheim. Hepes-buffered saline (HBS) is 10 mM Hepes, 0.15 M NaCl, 0.005% surfactant P20, pH 7.4. Buffer A is 10 mM Hepes, 0.15 M NaCl, 50 μM EDTA, 0.005% surfactant P20, pH 7.4. Buffer B is 20 mM Mops-NaOH, 20 mM KCl, 80 mM NaCl, 5 mM $MgCl_2$, pH 7.2. The synthetic hexahistidine peptide was obtained from Biomedical Centre (Uppsala University, Uppsala, Sweden).

GroEL and His-tagged GroES. GroEL was purified as described previously (28). The GroES gene was amplified by PCR from plasmid pOF39 (29) using oligonucleotides to introduce an *Rca*I site at the N-terminus and six histidines followed by a *Hin*dIII site at the C-terminus. After cleavage with *Rca*I and *Hin*dIII, the PCR product was cloned into pCKIPM (30). For GroES preparation, *E. coli* JM83 harboring the resulting plasmid pEShisC was grown at 37°C to OD_{550} 0.5 in 2× YT medium containing 100 μg/ml ampicillin, and the expression of GroES was induced with 1 mM isopropyl-β-D-thiogalactopyranoside (IPTG). After 10 h of induction, the cells were harvested by centrifugation, resuspended in HBS containing 0.1 mg/ml DNaseI, and passed through a French press. The resulting homogenate was centrifuged and the supernatant, mixed with imidazole (in HBS) to a final concentration of 20 mM, was loaded onto a Ni^{2+}–NTA superflow column (Qiagen) equilibrated with HBS. After washing the column first with HBS, then with 75 mM imidazole in HBS, GroES was eluted in a 75–500 mM imidazole gradient at an imidazole concentration of about 250 mM. The purity was analyzed by sodium dodecyl sulfate–polyacrylamide gel electrophoresis (SDS–PAGE) and visualized by Coomassie brilliant blue staining. The molecular weight was determined by electrospray mass spectrometry and found to be identical to the theoretical value.

Citrate synthase. This homodimer was purified with two His tags (CS-2His) (at the C-terminus of both subunits) and four His tags (CS-4His) (at the N- and the C-terminus of both subunits) as described elsewhere (5).

GrpE. The gene of this *E. coli* protein (a gift from Costa Georgopoulos, University of Geneva, Switzerland) was cloned by PCR into the *Hin*dIII and *Bam*HI restriction sites of the vector pQE9 (Qiagen). The protein, carrying an N-terminal hexahistidine tag, was expressed in *E. coli* and purified by IMAC on Ni^{2+}–NTA–agarose essentially as described for His-tagged GroES. The His-tagged protein was found to have the identical activity as wild type (wt) GrpE as a nucleotide exchange factor for the DnaK protein in an *in vitro* assay for molecular chaperone activity (31).

Maltose-binding protein. The *E. coli* maltose binding protein (MBP) was used in three variants, two of which carried one His tag at either the N- or the C-terminus and one which carried His tags at both the N- and the C-termini. The MBP coding sequence was derived from vector pMAL-c2 (New England Biolabs) and all three constructs used the vector pET-23a(+)

(Novagen), which puts transcription under the control of the T7 promoter. The proteins were expressed in *E. coli* BL21[pT7POL23] (32), in which T7 RNA polymerase itself is induced by a temperature shift from 30 to 42°C. All three MBP variants were expressed in soluble form and purified by IMAC as described for His-tagged GroES.

Glutathione S-transferase. C-terminally His-tagged glutathione *S*-transferase (GST) from *Shistosoma japonicum* was produced from vector pGEX-5X-2 (Pharmacia Biotech), modified by insertion of a hexahistidine encoding sequence into the multiple cloning site. The protein was expressed in soluble form in *E. coli* XL1-blue MR (Stratagene) and purified by IMAC as described above.

Streptavidin. Streptavidin (SA) homotetramer was obtained from Boehringer-Mannheim. The His tag was introduced by covalently linking the hexahistidine peptide via the NH_2-terminus to NHS-LC-Biotin (Pierce). The His_6–biotin was mixed in 10-fold molar excess with SA. His-tagged SA was separated by gel filtration from free peptide. Quantitative amino acid analysis indicated the presence of 4 mol of peptide per mole of SA.

N1–N2 domain of gIIIp of phage fd and the antibody scFv fragment FITC-E2. The monomeric proteins were purified with one His tag as described previously (30).

E. coli total protein extract. Strain BL21 carrying plasmid pUC19 was grown overnight in 1 liter of LB medium containing 100 μg/ml ampicillin. Cells were harvested, resuspended in 25 ml of 0.15 M NaCl, and disrupted by sonication. After clearing the lysate by centrifugation, the soluble protein extract was dispensed in aliquots and stored at −20°C.

Determination of the protein concentration. For all proteins, except GroEL and GroES, the extinction coefficient was calculated according to Gill and von Hippel (33) and the protein concentration was determined photometrically. Because of the low content of aromatic amino acids, the bicinchoninic acid assay (Pierce) was used to determine the concentration of GroEL and GroES.

Analysis of Sensor Chip NTA. The binding capacity was tested with a 7-min pulse of 500 nM hexahistidine peptide in running buffer (buffer A), following the optimized method for ligand binding as described below. To compare chips and binding conditions, the binding levels were determined 270 s after the end of the hexahistidine injection.

Experimental design. Most of the optimization experiments performed were based on statistical experimental design (34). In these designs, all factors (e.g., pH, NaCl concentration, and Tween 20 concentration) are varied uncorrelated and simultaneously at two to five levels using well-defined experimental plans. For instance, variation of the factor pH at three levels means that three different pH values were studied. The experiments are always performed in random order to avoid systematic errors. Regression analysis is initially used to identify the significant factors and the interaction effects between the factors and to rank their relative order of importance. A simple and informative way to display the results is to plot the response at the edges of a cube defined by the significant factors or simply by sorting the data table using the information obtained in the regression analysis.

Activation of the Sensor Chip NTA with nickel chloride. The dependence of the Ni^{2+} activation on variations in $NiCl_2$ concentration, contact time, pH, and NaCl concentration was tested by varying four levels at once in an experiment using an L9-array design (34). The immobilization level of GST was used as quality parameter.

The influence of variations in ligand buffer on the immobilization level of His-tagged proteins to the surface. The influence of the variations in ligand buffer on the immobilization level was studied using different ligands and experimental designs, varying NaCl concentration (0.05, 0.1, 0.15, and 0.2 M), pH (6.4, 6.9, 7.4, and 7.9), and Tween 20 concentration (0, 0.002, 0.005, and 0.008%). The immobilization level was measured for SA, GST, and hexahistidine peptide. The same concentrations of proteins and peptides were used throughout these experiments.

EDTA in running and ligand buffers. Contaminating metal ions in the running buffer and ligand buffer can influence the binding of the ligand to the Ni^{2+}–NTA surface. Experiments were performed where low concentrations of EDTA (0, 50, and 300 μM) were added to the running buffer. SA was the test protein and was diluted in the chosen running buffer. The dissociation of Ni^{2+} and His-tagged SA from the surface was measured as a decrease in signal (RU) during 10 min, and the apparent dissociation rate constant (k_{off}) was calculated using a monoexponential model for the dissociation.

Regeneration conditions. The robustness of the regeneration procedure against variations in EDTA concentration, contact time, and pH was tested in a nine-run 2^3-factorial design (34). The center point was run in triplicate, giving 11 experiments. GST was used as the test protein. Each of the 11 experiments (including activation, injection of ligand, and regeneration) was sequentially replicated 10 times. The relative level (%) of the baseline before and after the experiment for these 10 injections was taken as a measure of the completeness of regeneration.

Binding assay and data analysis of the GroEL/GroES system. Each binding cycle was performed with a constant flow of buffer B at 5 or 10 μl/min. First,

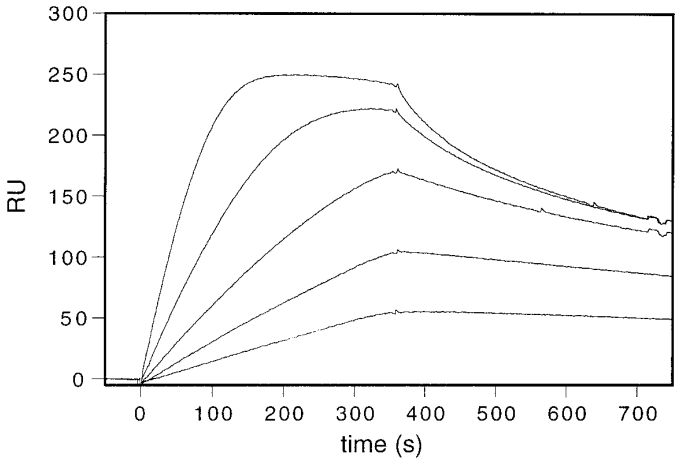

FIG. 1. Overlay plot showing the binding of the hexahistidine peptide at different concentrations (8, 15, 31, 62, and 125 nM) to the Ni^{2+}–NTA surface. At high concentrations (31, 62, and 125 nM) a rapid dissociation of the hexahistidine peptide was observed, whereas at low concentrations a stable binding was achieved, due to rebinding effects and possibly avidity (see text).

10 μl of $NiCl_2$ (500 μM) was injected onto the surface. Next, 10 to 50 μl GroES in HBS or buffer B was injected to generate a fresh immobilization in every cycle. The surface was then washed for 50 s with either HBS or buffer B. Samples of GroEL in buffer B containing no additive, 5 mM ADP, or 5 mM ATP were injected to study binding (association phase), and dissociation was effected by coinjection of buffer B containing no additive, 5 mM ADP, or 5 mM ATP. The surface was regenerated by injection of 0.35 M EDTA, pH 8.3, or 1 M imidazole, pH 7.0. The data analysis was carried out using the BIAevaluation 2.0 software (Biacore AB) and by global fitting analysis using the CLAMP program written by Morton and Myszka (35, 36).

RESULTS

Chip performance. Binding of hexahistidine peptide to the Ni^{2+}-activated NTA chip was used as a measure of the binding capacity (Fig. 1). The high level of Ni^{2+}-NTA derivatization is already apparent from the almost linear mass-transport limited on-rate and very strong rebinding, making the off-rate dependent on free Ni^{2+}–NTA sites and thus on injected peptide concentration (see below). To compare chips, the peptide concentration was chosen such that a further increase in concentration did not result in a significantly enhanced binding level, and the binding level was determined 270 s after the end of analyte injection. Despite the relatively small absolute values that can be obtained with such a low-molecular-weight ligand, this assay was shown to properly reflect variations in NTA levels by the absolute number of resonance units reached for every chip (data not shown). The Sensor Chip NTA used in this study had a hexahistidine peptide binding capacity in the range of 150 to 200 RU, while chips modified according to protocols described previously (16, 17) gave a binding level of about 100 RU. The coefficient of variation in binding levels between 25 chips from five different syntheses was 2.3% (data not shown).

Activation of the NTA surface with nickel chloride. The immobilization level of GST reaches a plateau at approx 2000 RU upon increasing the $NiCl_2$ concentration to about 300 μM (Table 1), while a further increase to 3000 μM has no further effect on the immobilization level. Thus, at the chosen $NiCl_2$ concentration of 500 μM and after a 1-min injection, all NTA sites are saturated with Ni^{2+}. These conditions for the activation of the NTA surface were used in all experiments, unless mentioned otherwise. The activation is stable against variations in pH, NaCl concentration, and contact time.

Variations of pH, NaCl concentration, and Tween concentration in the running and ligand buffers. The influence of the composition of ligand HBS buffer on the affinity of His-tagged ligands to Ni^{2+}-activated NTA was tested for GST, SA, and hexahistidine peptide. The difference between the lowest and highest immobilization level varied by a factor of 20 for GST, 3 for SA, and 1.1 for the hexahistidine peptide. As an example, the influence of pH, NaCl, and Tween on the immobilization level of SA is shown in Fig. 2. In this case an increase in pH and NaCl concentration decreases the immobilization level in a mutually dependent way. At pH 6.9 an increase in NaCl concentration decreases the immobilization level more than at pH 7.4 and 7.9. The influence of pH, NaCl, and Tween on the immobilization level of GST and the hexahistidine peptide was qualitatively the same as that for SA (data not shown). While Fig. 2 provides guidance for the optimal binding of the His tag, the binding of the immobilized ligand's interaction partner (the analyte) to the Ni^{2+}-activated

TABLE 1

The Influence of $NiCl_2$ Concentration, Contact Time, and pH on the Immobilization Level of GST

$NiCl_2$ (μM)	Contact time (min)	pH	NaCl (M)	Immobilized GST (RU)
30	0.3	6.4	0	25
30	1	8.4	0.5	17
30	4	7.4	0.15	229
300	0.3	7.4	0.5	1999
300	1	6.4	0.15	2023
300	4	8.4	0	1945
3000	0.3	8.4	0.15	2008
3000	1	7.4	0	2174
3000	4	6.4	0.5	2123

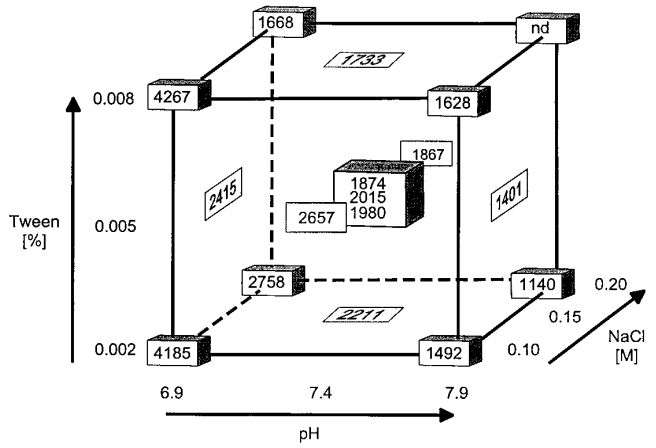

FIG. 2. Cube plot showing the immobilization level of streptavidin (100 nM) at different ligand buffer compositions. Three different parameters are plotted in three dimensions. The central value (pH 7.4, 0.15 M NaCl, 0.005% Tween) was determined in triplicate. For streptavidin the pH has the strongest influence on the immobilization level.

NTA surface must also be checked, and this should be as low as possible. This may require some compromise in conditions, and Fig. 2 should prove to be helpful for this purpose.

EDTA in running and ligand buffers. The addition of 50 μM EDTA in the running buffer to scavenge contaminating ions does not influence the Ni^{2+} activation of the NTA surface (Table 2). The differences in immobilization levels of His-tagged proteins are negligible in all model systems studied when EDTA in concentrations from 0 to 50 μM is added (Table 2). When the EDTA concentration was increased to 300 μM, however, a significant decrease in the immobilization level of His-tagged SA was observed (Table 2).

Concentration of His-tagged ligand and number of His tags. In Fig. 3a, an overlay plot of binding and dissociation of CS-4His at concentrations of 25 and 50 nM is shown. At higher protein concentrations (for the proteins tested, around 50 to 200 nM), multiphasic binding curves, characterized by a drop in binding level during the injection phase (data not shown) and less stable binding, were observed (cf. Fig. 1). This indicates that the intrinsic affinity of the His tag to Ni^{2+}–NTA is low and requires continuous rebinding to neighboring sites to generate stable binding. At high immobilization levels, not all protein molecules will have full access to enough free Ni^{2+}–NTA sites for efficient rebinding, and thus higher dissociation rates will be observed (see Fig. 3a). This concentration dependence of apparent off-rates is also observed for the hexahistidine peptide (Fig. 1).

A prerequisite for measuring the kinetics of binding of further partners (analytes), interacting with the immobilized protein on the NTA surface, is that the binding of the first protein to the surface is very stable. We tested several proteins with differences in position and number of His tags for their binding to the Ni^{2+}–NTA surface (Table 3). In Fig. 3b, an overlay plot of five different proteins is shown. GroES has seven subunits, but consists of about 20% chromosomally encoded wt GroES, as shown by SDS–PAGE, and thus carries only five to six His tags per heptamer. This protein is bound very tightly and no dissociation can be detected (Fig. 3b, curve 1, and Table 3). GrpE is a homodimer in solution (37) and also binds without any dissociation over a long time period (Fig. 3b, curve 4, and Table 3). The third protein studied for stable binding is citrate synthase (CS), also a homodimeric protein. Its structure shows that both N-termini are located on opposite

TABLE 2

The Influence of EDTA in Running and Ligand Buffers on Protein Binding to the NTA Chip

Ligand	Concentration (μM)[a]	EDTA (μM)[b]	Immobilized ligand (RU)	k_{off} (10^{-4} s^{-1})[c]	Dissociation (RU)[d]
Ni^{2+}	500	50	61	nd	nd
Streptavidin	0.10	0	1633	1.26	121
Streptavidin	0.10	50	1546	1.33	122
Streptavidin	0.10	300	1337	1.70	132
GroES	0.03	0	1552	nd	nd
GroES	0.03	50	1601	nd	nd
CS-4His	0.06	0	3691	nd	nd
CS-4His	0.06	50	3642	nd	nd
GrpE	0.15	0	3356	nd	nd
GrpE	0.15	50	3312	nd	nd

Note. nd, no dissociation detectable.
[a] Ligand concentration used in the immobilization experiment.
[b] EDTA concentration in running and ligand buffer.
[c] Apparent dissociation rate constant for the dissociation of the immobilized protein from the surface.
[d] Decrease in signal 10 min after injection was completed.

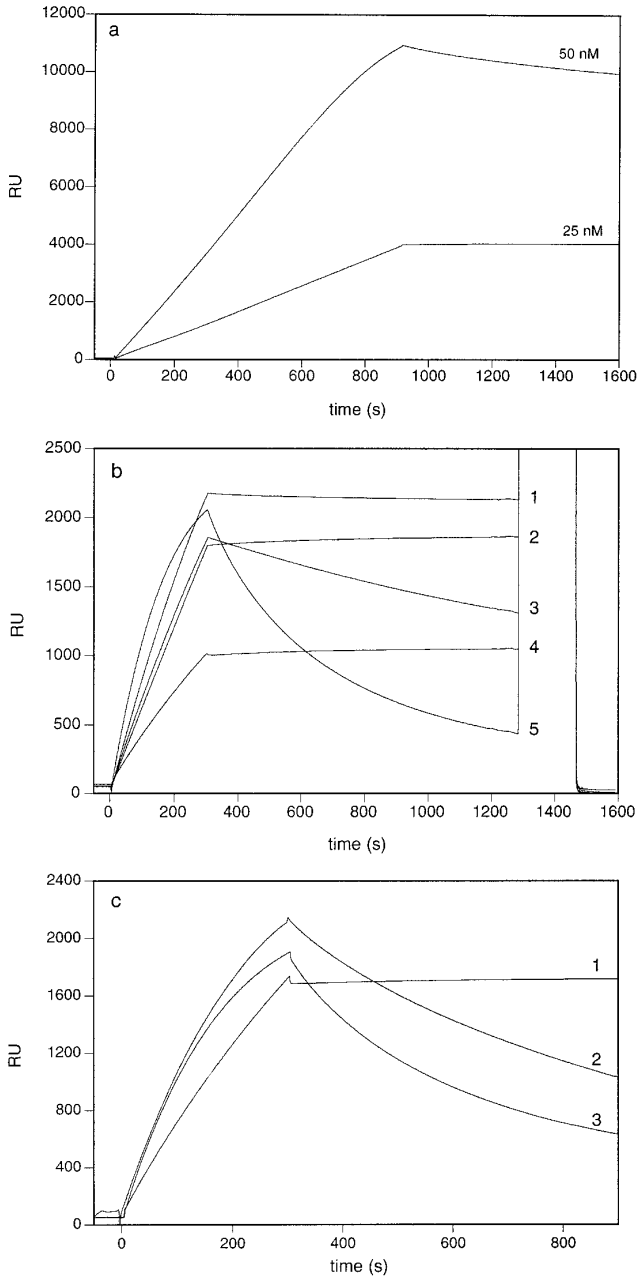

FIG. 3. (a) Overlay plot showing binding of CS-4His to the Ni^{2+}–NTA surface at two different concentrations (25 and 50 nM). The amount of protein bound to the surface was chosen very high (more than 10000 RU) to show that at high protein concentrations (in this case 50 nM), where the Ni^{2+}–NTA sites become saturated, even proteins with four His tags dissociate from the surface, due to the loss of rebinding. At lower concentrations (less than 25 nM), binding was totally stable. (b) Overlay plot of five different proteins, with different numbers of His tags, binding to the same Ni^{2+}–NTA surface. Curve 1 is GroES, curve 2 is CS-4His, curve 3 is CS-2His, curve 4 is GrpE, and curve 5 is MBP. The number and the position of the His tags, as well as the protein concentrations used in the experiment, are summarized in Table 3. The regeneration of the Ni^{2+}–NTA surface (from 1300 to 1500 s) was carried out with 0.35 M EDTA, pH 8.3. (c) Overlay plot of three variants of MBP. All were injected for the same length of time using the same concentration of 120 nM. Both mono

sides of the molecule (38), and the same is true for the C-termini. It seems likely that the two C-terminal His tags are not accessible simultaneously for binding to the Ni^{2+}–NTA surface, and consistent with this assumption, the protein was found to dissociate quite rapidly (Fig. 3b, curve 3, and Table 3). In contrast, CS with both N-terminal and C-terminal His tags (carrying a total of four His tags) is immobilized very stably to the sensor chip surface (Figs. 3a and 3b, curve 2, and Table 3). An example of a predominantly monomeric protein is MBP, which is released very rapidly from the surface (Fig. 3b, curve 5). We then compared the stability of binding of MBP with a His tag at the C-terminus, the N-terminus, or at both ends. In Fig. 3c, it is shown that no stable binding could be achieved for either variant with only one His tag, but MBP with His tags on both the N- and the C-terminus gives stable binding.

The results obtained with the two monomeric MBP variants are at variance with results reported by Gershon and Khilko (17). These authors observed stable binding for a presumably monomeric protein with only one His tag to the Ni^{2+}–NTA surface at pH 7.0. Since our surface shows twice the capacity for the hexa-histidine peptide than that described by Gershon and Khilko (17) (Fig. 1), such stable binding of a monomeric protein with only one His tag should also be observable. We therefore tested two further monomeric proteins with only one His tag for stable binding, namely the N1–N2 domain of gIIIp of phage fd (39) and the anti-fluorescein antibody scFv fragment FITC-E2 (39, 40). For both proteins, gel filtration showed the molecular weight expected for monomers (data not shown). In Fig. 4a the immobilization of N1–N2 at a flow rate of 25 μl/min is shown, and no stable binding could be achieved. We can estimate the K_D value for the binding of the His tag in N1–N2 to the Ni^{2+}–NTA surface to be about 7×10^{-7} M at pH 7.0, using the global fit program CLAMP (35, 36) for the calculation. A two-compartment model was used to describe mass transport (15, 36). Due to the strong rebinding during the dissociation and due to the very dense coating of NTA, the affinity might be even weaker than 7×10^{-7} M. When raising the pH to 8.3 the dissociation rate is decreased slightly, but still no stable binding is observed (Fig. 4b). With the antibody scFv fragment FITC-E2, no stable binding could be achieved at pH 7.0 (Fig. 4c). However, as shown in Figs. 4b and 4c, the flow rate also has an influence on the measured dissociation, since at 5 μl/min the dissociation rate is slower than at 25 μl/min, further indicating the impor-

His-tagged variants dissociated rapidly. Curve 2 is N-terminally His-tagged MBP and curve 3 is C-terminally His-tagged MBP. The variant with the N- and the C-terminal His tag bound stably to the Ni^{2+}–NTA surface (curve 1).

TABLE 3

Summary of Proteins Shown in Fig. 3b

Curve number	Protein	MW[a] (kDa)	Position of His tag	Form	Number of His tags[b]	Conc. (nM)[c]
1	GroES	10	C	Heptamer	5–6[d]	40
2	CS-4His	80	C + N	Homodimer	4	15
3	CS-2His	80	C	Homodimer	2	30
4	GrpE	26	N	Homodimer	2	60
5	MBP	43	C	Monomer	1	120

[a] Molecular weight for the monomer.
[b] Total number of His tags per oligomer.
[c] Protein concentration in the immobilization experiment.
[d] GroES carries only 5–6 His tags, because about 20% of the protein is chromosomally encoded wt GroES and about 80% is plasmid encoded His-tagged GroES, as determined by SDS–PAGE and electrospray mass spectrometry.

tance of rebinding in the observed phenomena. At pH 8.3, when only 80 RUs are coupled and a flow of 5 μl/min is used, the scFv fragment binds stably to the surface (Fig. 4d). Thus, stable binding of monomeric proteins is not a general phenomenon, but protein-dependent and very sensitive to pH and flow rate. We also attempted to determine the binding constant of the hexahistidine peptide to Ni^{2+}–NTA (Fig. 1), using a

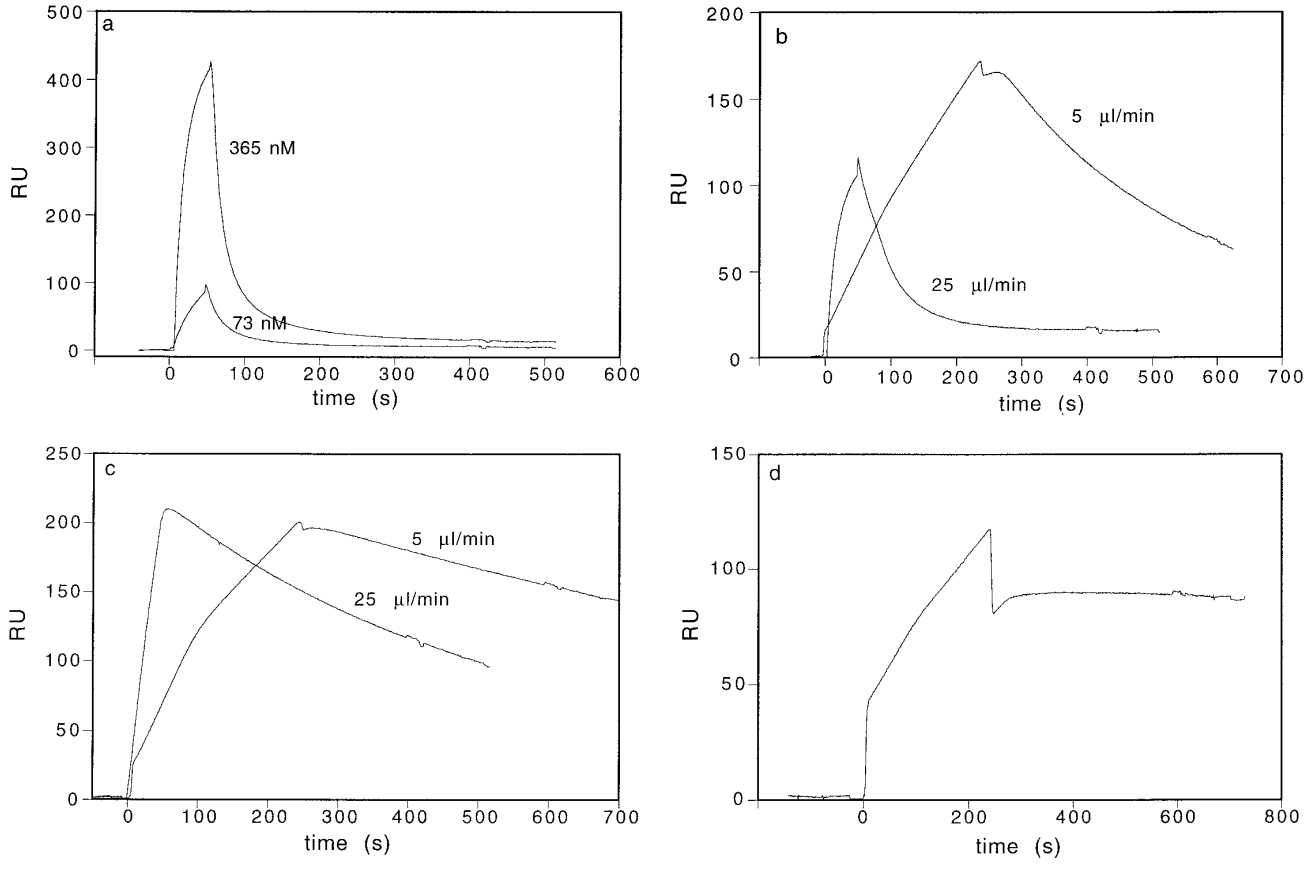

FIG. 4. (a) Overlay plot showing the binding of the N1–N2 domain of phage fd at two different concentrations (73 and 365 nM) to Ni^{2+}–NTA. The pH was 7.0 and the flow rate was 25 μl/min. (b) Overlay plot showing the binding of the N1–N2 domain (73 nM) to Ni^{2+}–NTA at pH 8.3. The binding was measured at two different flow rates (5 and 25 μl/min). (c) Overlay plot showing the binding of the scFv fragment FITC-E2 (26 nM) to Ni^{2+}–NTA at two different flow rates (5 and 25 μl/min) at a pH of 7.0. (d) A plot showing the binding of the scFv fragment FITC-E2 (26 nM) to Ni^{2+}–NTA at pH 8.3 with a flow rate of 5 μl/min.

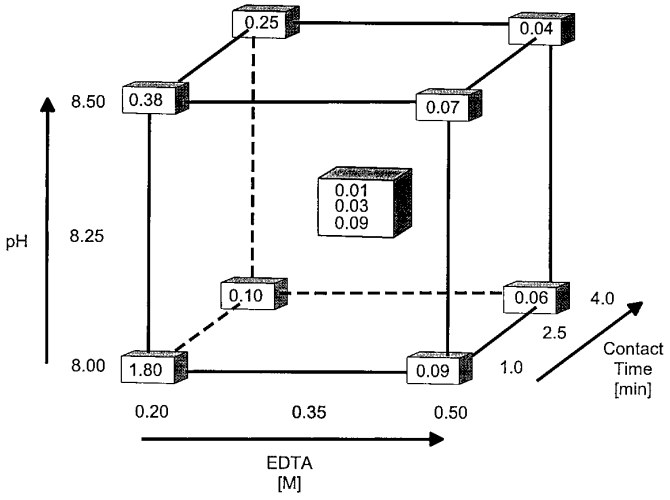

FIG. 5. Cube plot showing the regeneration conditions tested with GST bound to the Ni^{2+}–NTA surface. The numbers given are the baseline change (in percentages) between the values before Ni^{2+} and GST injection and after regeneration. A small value indicates complete regeneration. The central values (pH 8.25, 0.35 M EDTA, 2.5 min contact time) were measured in triplicate.

global fit and a rebinding model (15, 35, 36). While the data are consistent with micromolar affinity, the rebinding is so strong that the simple two-compartment model for mass transport and rebinding leaves nonrandom residuals, precluding an exact determination.

Regeneration of the NTA chip. Regeneration is one of the crucial steps in every experiment using BIACORE instruments. A reproducible reuse of the surface is important for the correct measurement of kinetics in concentration series. For the Ni^{2+}–NTA surface the known eluents from IMAC can be used. For example, GST immobilized to the Ni^{2+}–NTA surface was eluted with EDTA as the regeneration reagent. In Fig. 5, a cube plot is shown, where the effects of pH, contact time, and EDTA concentration on the regeneration are shown. The baseline levels before the Ni^{2+} injection and after the regeneration step were compared, and the relative baseline variation in these 11 experiments was very low (<0.4%). Only when low EDTA concentrations, short contact times, and low pH were combined, the baseline variation increased to about 1.8%. With pH 8.3, 3 min of contact time, and 0.35 M EDTA (our recommended conditions), the baseline level after each cycle was found to be very stable.

In chromatography, imidazole is frequently used as eluent. An imidazole concentration of 50 mM was found to give a complete dissociation of GrpE (2000 RU) from the surface. Repeated binding and regeneration cycles without renewed Ni^{2+} injection resulted in decreasing binding levels due to loss of some Ni^{2+} in each cycle (data not shown). This is also known from chromatography, where the Ni^{2+} has to be replenished after several purification runs.

Interactions of GroEL and GroES. As an example of an interesting biological system, which can be studied conveniently with the NTA chip, we investigated the interaction between GroEL and GroES, the components of the *E. coli* chaperonin system. GroES was expressed in the cytoplasm of *E. coli* with six histidines fused to the C-terminus. The purified protein consists of about 80% His-tagged GroES (from the plasmid-encoded gene) and of about 20% wt GroES (from the chromosome).

Binding of GroEL to GroES only occurs in the presence of nucleotides (23). Binding is followed by K^+-dependent ATP hydrolysis on GroEL subunits in the bound ring (41). To rule out any unspecific binding of GroEL to the Ni^{2+}–NTA surface or to His-tagged GroES, GroEL was injected without any nucleotide onto the GroES Ni^{2+}–NTA surface. No binding of GroEL was observed (Fig. 6a, inset). Also for ATP alone, which might bind to Ni^{2+} due to the negatively charged phosphates, no binding to the GroES Ni^{2+}–NTA complex was observed (data not shown). Figure 6b shows GroEL binding to GroES with ADP present during the association phase, as well as during the dissociation phase. No dissociation was detectable (Table 4), which is consistent with the hypothesis that ATP hydrolysis is required for liberation of GroES (41). In Fig. 6c ATP was present in both association and dissociation phases. A 10-fold acceleration in the on-rate (Table 4) and about a 5000-fold faster off-rate were determined compared to the dissociation rate in the presence of ADP (Figs. 6b and 6c). To confirm the acceleration of the dissociation, ADP was used during the association phase, and ATP was added during the dissociation phase (Fig. 6d). A clear dissociation is visible when ATP was added only during the dissociation phase.

Recently two studies of the kinetics of GroEL/GroES complex formation and dissociation using the BIACORE instrument have been reported (25, 26). In these studies the calculated on-rate and off-rate in the presence of ATP were determined to be faster than those in the presence of ADP, which is in agreement with our results. Our data analysis was first carried out using the BIAevaluation software 2.0, as used in the above cited studies. The resulting rates are in good agreement with the previously published values, but the resulting fits were not very satisfactory. Therefore, we used global fitting analysis (35, 36) instead. However, a simple 1:1 model, even when including mass transport limitation, still does not describe the data correctly. The fit is improved if a model including mass transport limitation and a heterogeneous surface (two types of complexes with different parameters) are assumed, but the kinetics of the chaperonin system seems

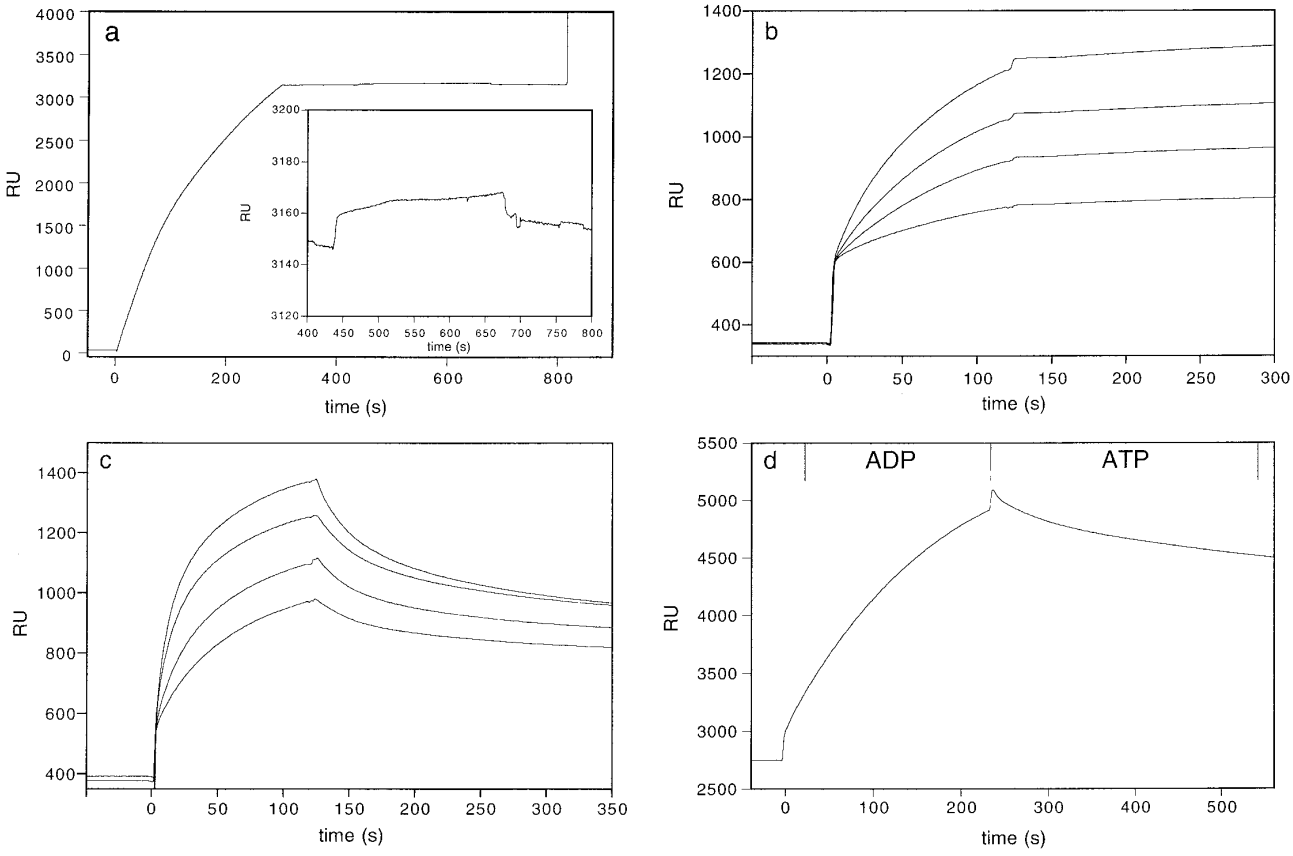

FIG. 6. (a) His-tagged GroES (38 nM) was injected onto a Ni^{2+}–NTA surface, resulting in about 3000 RUs, followed by a GroEL (65 nM) injection (420 to 670 s, inset in Fig. 6a) without addition of any nucleotide to test the unspecific binding of GroEL to the Ni^{2+}–NTA surface and to GroES. (b and c) Overlay plots of the association and dissociation of GroEL and GroES in the presence of ADP (b) and ATP (c). GroES (19 nM) was injected onto a Ni^{2+}–NTA surface, resulting in about 300 RUs. The nucleotides, used in a 5 mM final concentration, were premixed with different concentrations of GroEL (13, 32, 65, and 130 nM) and finally injected onto the GroES surface. The regeneration was carried out with 0.35 M EDTA, pH 8.3. (d) 38 nM His-tagged GroES was immobilized (2500 RUs) and the binding of GroEL (65 nM) was measured in the presence of 5 mM ADP. During the dissociation phase, 5 mM ATP was present in the running buffer.

far more complicated and does not warrant a K_D determination at this point. The off-rate estimated from the double exponential fit is very similar to k_{cat} for ATP hydrolysis by GroEL (41, 42). However, further studies are required to kinetically describe this system in detail. We can note, however, that the same shape of association and dissociation phase is observed in all three BIACORE studies of the GroEL/ES system. Since the results from covalent coupling and noncovalent immobilization presented here closely agree, we can conclude that the His tag does not interfere with the functionality of the protein and that the GroES multimers containing five to six His tags are identical in their biological behavior to the wt GroES homoheptamers without His tags.

TABLE 4

Kinetic Parameters of GroEL and GroES Interaction in the Presence of ATP and ADP at 25°C

Nucleotide	k_{on1} (M^{-1} s^{-1})	k_{on2} (M^{-1} s^{-1})	k_{off1} (s^{-1})	k_{off2} (s^{-1})
ATP[a]	1.3×10^6	1.5×10^5	1.1×10^{-2}	7.5×10^{-4}
ADP	1.6×10^5		nd	

Note. nd, not determined.

[a] Global fit (35, 36), using two on- and off-rates, as well as mass transport limitation ($k_{tr} = 3.4 \times 10^{-6}$ m/s).

Crude samples. A feature of the NTA surface is that it should be possible to use *E. coli* cell lysate, containing the His-tagged protein of interest, for immobilization, because the Ni^{2+}–NTA surface should itself act as an IMAC column. Since it is known that some proteins bind unspecifically to Ni^{2+}–NTA, we tested *E. coli* cell lysates for "background" binding to the Ni^{2+}-activated NTA surface. The observed background binding must be nickel related, because no binding occurred without prior nickel activation, and all bound protein could be

TABLE 5

Effect of $NiCl_2$ on Immobilized Proteins

$NiCl_2$ (μM)	Immobilization level before and after $NiCl_2$ injection (RU)					
	GroES		GrpE		CS-4His	
	$-NiCl_2$	$+NiCl_2$	$-NiCl_2$	$+NiCl_2$	$-NiCl_2$	$+NiCl_2$
0	1083	1082	665	666	790	710
250	1070	1071	660	140	763	363
1000	1083	1095	670	50	807	307

eluted with 0.35 M EDTA (data not shown). However, addition of $NiCl_2$ to a final concentration of 250 μM to *E. coli* lysate prior to injection reduced background binding to about half. There was a clear variation between proteins in the effect of $NiCl_2$ injected on the immobilized proteins: Whereas immobilized GroES was unaffected by an injection of 1 mM $NiCl_2$, both GrpE and CS-4His dissociated rapidly at 250 μM $NiCl_2$ (Table 5). This may indicate the strength of the interaction of the immobilized proteins, as free Ni^{2+} will compete with the immobilized Ni^{2+} on the chip for binding to the His tag.

Figure 7 shows a sensorgram, where an *E. coli* crude extract, containing His-tagged GroES, was injected onto the Ni^{2+}–NTA surface. A rapid decrease of the signal, due to the many different nonbinding proteins or immediate dissociation of very weakly bound proteins in this mixture, was observed directly after injection. This was followed by a residual level of stable binding, indicating specific binding of GroES to the Ni^{2+}–NTA surface. To verify that the remaining signal is indeed due to GroES, GroEL was injected in the presence of ADP. The response levels of GroEL, relative to immobilized GroES, were comparable with the levels obtained with purified GroES in Fig. 6. A slight dissociation is detectable, which might be due to the fact that about 10-fold more GroES was immobilized. Alternatively, some ATP from the crude extract may still be present, which would lead to an observable dissociation, as shown in Fig. 6. As a further control a crude *E. coli* extract containing GroES without His tag was injected, followed by a GroEL + ADP injection, but no binding of GroEL could be observed (data not shown).

DISCUSSION

The binding of His-tagged protein ligands to the Ni^{2+}–NTA surface needs to be very stable, if kinetics of interactions between the immobilized protein (the ligand) and a further partner (the analyte) are to be studied. In contrast to the very high affinity of the metal ion to NTA, the His tag binds only with low affinity to the Ni^{2+}–NTA complex. We estimate the dissociation constant to be about 10^{-6} M. While this is convenient for chromatography, as it allows mild elution, the immobilization method may at first seem less well suited for immobilization, a prerequisite for studying protein–protein interactions. Nevertheless, we show here that such kinetic measurements are possible.

Interestingly, stable binding can be reached for the monomeric hexahistidine peptide but not for monomeric His-tagged proteins. Because of its small size and its flexibility, the peptide may have access to more Ni^{2+}–NTA binding sites, thus facilitating rebinding. It may even be possible to bind simultaneously to two closely spaced Ni^{2+}–NTA sites at once (Fig. 1). At higher concentrations, when free binding sites are scarce, a clear dissociation is visible. The dissociation does not follow a single exponential, and the baseline level is not reached during the dissociation phase. These are clear indications for rebinding. The rebinding within the Ni^{2+}–NTA–dextran matrix is an important factor to reach stable binding and thus a very useful property of the system in this application. Furthermore, since correct kinetic analysis of the binding of an analyte to its immobilized ligand depends on using a low ligand density, it is very convenient to simply use low concentrations of the ligand for immobilization.

Proteins with only one His tag only bind very weakly to the Ni^{2+}–NTA surface at neutral pH. The binding is improved at very low flow rates and at high pH. However, these conditions are not very suitable for kinetic measurements, because only high flow rates reduce mass transport limitation and rebinding (43).

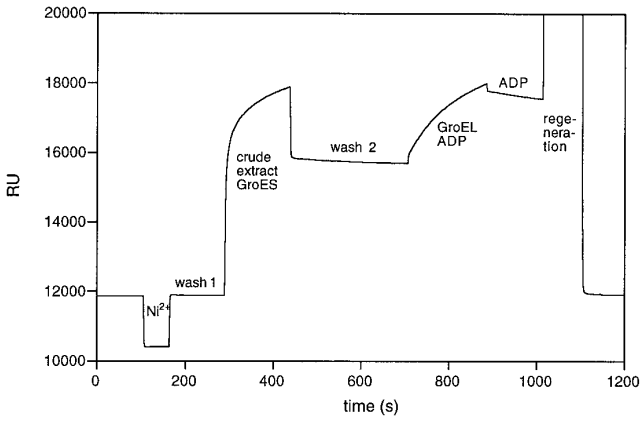

FIG. 7. Binding of GroEL to GroES, where GroES has been immobilized unpurified, directly from an *E. coli* crude extract. The NTA surface was activated with $NiCl_2$ (Ni^{2+}) and washed with HBS buffer (wash 1), and about 45 RU of Ni^{2+} was bound to NTA. An *E. coli* crude extract, containing His-tagged plasmid-encoded GroES (crude extract GroES), was injected onto the Ni^{2+}–NTA surface. A washing step with HBS buffer (wash 2) followed. GroEL (65 nM) in the presence of 5 mM ADP was injected (GroEL/ADP). The dissociation was measured in the presence of 5 mM ADP. Regeneration was carried out as described in the legend to Fig. 6.

A pragmatic solution to increase stability of ligand binding to Ni^{2+}–NTA is to take advantage of an avidity effect. With two His tags, either from a homodimer or from two His tags in a monomer, stable binding can be achieved due to simultaneous binding of the two His tags. This is shown here for MBP, GrpE, and GST. For CS-2His, however, only a limited avidity effect could be achieved, which might be due to the relative location of the termini on opposite sides of the molecule. The proteins in this study which carried more than two His tags, SA and GroES, both exhibited stable binding.

The binding of the His-tag to the Ni^{2+}-NTA surface is affected by different parameters, e.g., Ni^{2+} activation, ligand and running buffer composition, ligand concentration, and regeneration conditions. We investigated all of them and describe a detailed protocol for the immobilization of His-tagged proteins. This optimized methodology was tested on seven different His-tagged proteins with good results.

Our results show that a maximal immobilization level is reached using a $NiCl_2$ concentration of 300 μM. We also show that the addition of 50 μM EDTA to the ligand and running buffers increases the assay stability without influencing the dissociation rate of the ligand from the surface. The presence of EDTA in the ligand or running buffer is an important factor to consider since EDTA is often used to inhibit metalloproteases in *E. coli* crude extracts and, for this reason, is also often added to purified samples to prevent degradation. The addition of EDTA eliminates contaminating ions in the ligand and running buffers, which could compete by binding to the protein or to free NTA sites. A reproducible immobilization level of Ni^{2+} of 40 to 60 RU is a good indication of a properly working surface. By varying the pH, NaCl, and surfactant concentrations we could change the immobilization level by a factor of 2 to 20, depending on the protein to be bound.

The complete regeneration of the NTA surface to the baseline level can be achieved with 0.35 M EDTA at pH 8.3, using a contact time of 3 min. This optimized regeneration methodology has now been tested on seven different proteins. Up to 100 regenerations have been carried out without significantly affecting the surface capacity. This also means that the same flow cell can be used for many different proteins.

As an example of an interesting system on which to test the performance of the NTA chip we chose the *E. coli* chaperonin system GroEL and GroES. The regeneration conditions for the chip allowed us to completely regenerate the surface after each cycle, and GroES was injected freshly for every cycle, ensuring retention of activity in every cycle. The data obtained with His-tagged GroES strengthen the biochemical studies, where K^+-ATP-dependent hydrolysis had been shown to be required for the release of GroES (41). The differences in the off-rates between ADP and ATP, present during dissociation, clearly show that only ATP can promote dissociation. Further work is required to untangle the kinetic complexities of the GroEL/ES system, as monoexponential behavior does not describe the kinetics satisfactorily, not even when mass transport limitations are taken into account.

In conclusion, the new NTA chip can be used conveniently for kinetic measurements using His-tagged proteins. The only limitation is that one His tag on a monomeric protein is usually not sufficient for stable binding, except in some special cases. However, even with a monomeric protein, a qualitative interaction analysis will be possible at low ligand concentrations. Immobilization and regeneration of the surface are both easier and more predictable than in the traditional covalent immobilization. The NTA surface also permits the replacement of the immobilized ligand in every cycle. This is a very important consideration for ligands which may be destroyed by the regeneration procedure, e.g., at low pH. Finally, the orientation of the immobilized ligand is predictable and homogenous. Even for nonpurified proteins the NTA surface can be used for qualitative kinetic analysis, provided controls of the background proteins are included, because of the high selectivity of binding. In conclusion, in cases where a His tag has no influence on the protein activity and function, the introduction of a His tag simultaneously simplifies purification (2, 4, 5), detection (6, 7), and also kinetic analysis with BIACORE instruments.

ACKNOWLEDGMENTS

We thank Dr. Alexander Szabo, Biacore AB USA, for providing the GrpE protein and for helpful discussions. We also thank Drs. Peter Lindner, Frank Hennecke, and Falk Schwesinger, University of Zürich, for providing citrate synthase, N1–N2 domain, and scFv FITC-E2.

REFERENCES

1. Nygren, P. Å., Stahl, S., and Uhlén, M. (1994) *Trends Biotechnol.* **12,** 184–188.
2. Hochuli, E., Bannwarth, H., Döbeli, R., Gentz, R., and Stüber, D. (1988) *Bio/Technology* **6,** 1321–1325.
3. Arnold, F. H. (1991) *Bio/Technology* **9,** 151–156.
4. Porath, J., Carlsson, J., Olsson, I., and Belfrage, G. (1975) *Nature* **258,** 598–599.
5. Lindner, P., Guth, B., Wülfing, C., Krebber, C., Steipe, B., Müller, F., and Plückthun, A. (1992) *Methods* **4,** 41–56.
6. Botting, C. H., and Randall, R. E. (1995) *BioTechniques* **19,** 362–363.
7. Lindner, P., Bauer, K., Krebber, A., Nieba, L., Kremmer, E., Krebber, C., Honegger, A., Klinger, B., Mocicat, R., and Plückthun, A. (1997) *BioTechniques* **22,** 140–149.
8. Karlsson, R., Michaelsson, A., and Mattsson, L. (1991) *J. Immunol. Methods* **145,** 229–240.
9. Colas, C. B., Jessen, T., Grishina, I., McCoy, J., and Brent, R. (1996) *Nature* **380,** 548–550.

10. Johnsson, B., Löfås, S., and Lindquist, G. (1991) *Anal. Biochem.* **198,** 268–277.
11. Barberis, A., Pearlberg, J., Simkovich, N., Farrell, S., Reinagel, P., Bamdad, C., Sigal, G., and Ptashne, M. (1995) *Cell* **81,** 359–368.
12. Karlsson, R., and Ståhlberg, R. (1995) *Anal. Biochem.* **228,** 274–280.
13. Nieba, L., Krebber, A., and Plückthun, A. (1996) *Anal. Biochem.* **234,** 155–165.
14. O'Shannessy, D., and Winzor, D. J. (1996) *Anal. Biochem.* **236,** 275–283.
15. Schuck, P. (1996) *Biophys. J.* **70,** 1230–1248.
16. Frostell Karlsson, Å., Johnson, B., and Panayotou, G. (1994) Proceedings, Fourth European BIAsymposium, Heidelberg, Germany, pp. 39–44.
17. Gershon, P. D., and Khilko, S. (1995) *J. Immunol. Methods* **183,** 65–76.
18. O'Shannessy, D. J., O'Donnell, K. C., Martin, J., and Brigham-Burke, M. (1995) *Anal. Biochem.* **229,** 119–124.
19. Sigal, G. B., Bamdad, C., Barberis, A., Strominger, J., and Whitesides, G. M. (1996) *Anal. Chem.* **68,** 490–497.
20. Hemmingsen, S. M., Woolford, C., van der Vies, S. M., Tilly, K., Dennis, D. T., Georgopoulos, C. P., Hendrix, R. W., and Ellis, R. J. (1988) *Nature* **333,** 330–334.
21. Chen, S., Roseman, A. M., Hunter, A. S., Wood, S. P., Burston, S. G., Ranson, N. A., Clarke, A. R., and Saibil, H. R. (1994) *Nature* **371,** 261–264.
22. Braig, K., Otwinowski, Z., Hegde, R., Boisvert, D. C., Joachimiak, A., Horwich, A. L., and Sigler, P. B. (1994) *Nature* **371,** 578–586.
23. Hunt, J. F., Weaver, A. J., Landry, S., Gierasch, L., and Deisenhofer, J. (1996) *Nature* **379,** 37–45.
24. Roseman, A. M., Chen, S., White, H., Braig, K., and Saibil, H. R. (1996) *Cell* **87,** 241–251.
25. Hayer-Hartl, M. K., Martin, J., and Hartl, F. U. (1995) *Science* **269,** 836–841.
26. Kawata, Y., Hongo, K., Nosaka, K., Furutsu, Y., Mizobata, T., and Nagai, J. (1995) *FEBS Lett.* **369,** 283–286.
27. Saibil, H. R. (1996) *Structure* **4,** 1–4.
28. Harris, J. R., Plückthun, A., and Zahn, R. (1994) *J. Struct. Biol.* **112,** 216–230.
29. Fayet, O., Ziegelhoffer, T., and Georgopoulus, C. (1989) *J. Bacteriol.* **171,** 1379–1385.
30. Krebber, C. (1996). PhD thesis, University of Zürich.
31. Szabo, A., Langer, T., Schroeder, H., Flanagan, J., Bukau, B., and Hartl, F. U. (1994) *Proc. Natl. Acad. Sci. USA* **91,** 10345–10349.
32. Mertens, N., Remaut, E., and Fiers, W. (1995) *Bio/Technology* **13,** 175–179.
33. Gill, S. C., and von Hippel, P. H. (1989) *Anal. Biochem.* **182,** 319–326.
34. Haaland, P. D. (1989) Experimental Design in Biotechnology, Dekker, New York/Basel.
35. Morton, T. A., Myszka, D. G., and Chaiken, I. M. (1995) *Anal. Biochem.* **227,** 176–185.
36. Myszka, D. G., Arulanantham, P. R., Sana, T., Wu, Z., Morton, T. A., and Ciardelli, T. L. (1996) *Prot. Sci.* **5,** 2468–2478.
37. Schönfeld, H.-J., Schmidt, D., Schröder H., and Bukau B. (1995) *J. Biol. Chem.* **270,** 2183–2189.
38. Remington, S., Wiegand, G., and Huber, R. (1982) *J. Mol. Biol.* **158,** 111–152.
39. Krebber, C., Spada, S., Desplanq, D., Krebber, A., Ge, L., and Plückthun, A. (1997) *J. Mol. Biol.* **268,** 607–618.
40. Vaughan, T. J., Williams, A. J., Pritchard, K., Osbourn, J. K., Pope, A. R., Earn-show, J. C., McCafferty, J., Hodits, R. A., Wilton, J., and Johnson, K. S. (1996) *Nature Biotechnol.* **14,** 309–314.
41. Todd, M. J., Viitanen, P. V., and Lorimer, G. H. (1994) *Science* **265,** 659–666.
42. Aharoni, A., and Horovitz, A. (1996) *J. Mol. Biol.* **258,** 732–735.
43. Myszka, D. G. (1997) *Curr. Opin. Biotechnol.* **8,** 50–57.